BULLETIN OF THE POLISH ACADEMY OF SCIENCES
TECHNICAL SCIENCES, Vol. 66, No. 6, 2018
DOI: 10.24425/bpas.2018.125944

Decoupling control for permanent magnet in-wheel motor using internal model control based on back-propagation neural network inverse system

Y. LI[1,2]*, B. ZHANG[2] and X. XU[1,2]

[1]Automotive Engineering Research Institute, Jiangsu University, Zhenjiang, 212013, China
[2]School of Automotive and Traffic Engineering, Jiangsu University, Zhenjiang, 212013, China

Abstract. The permanent magnet in-wheel motor (PMIWM) is a nonlinear, multivariable, strongly coupled and highly complex system. The key to the development and application of the PMIWM consists in the improvement of its control accuracy and dynamic performance. In order to effectively decouple the PMIWM, this paper presents a novel internal model control (IMC) approach based on the back-propagation neural network inverse (BPNNI) control method. First, theoretical analysis is conducted to show the existence of the PMIWM inverse system, to be modeled mathematically. The inverse system approximated and identified by the back-propagation neural network (BPNN) constitutes the back-propagation neural network inverse (BPNNI) system. Then, by cascading the BPNNI system on the left side of the original PMIWM system, a new decoupling, pseudo-linear system is established. Moreover, the 2-DOF internal model control (IMC) method is employed to design the extra closed-loop controller that further improves disturbance rejection and robustness of the whole system. Consequently, the proposed decoupling control approach incorporates the advantages of both the BPNNI and the IMC. Effectiveness of thus proposed control approach is verified by means of simulation and real-time hardware-in-the-loop (HIL) experiments.

Key words: electric vehicle, permanent magnet in-wheel motor, back-propagation neural network, inverse system, internal model control.

1. Introduction

Recently, the in-wheel motor driven electric vehicle (EV) has developed rapidly as a new energy and environment-friendly transportation alternative, thanks to its high efficiency, non-pollution, low noise and a variety of other characteristics. Differing from the traditional driving manner, the in-wheel motor drives the wheels directly. Thus, the in-wheel motor driven EV has unique advantages, such as simple and compact structure, high energy efficiency and independent torque control [1, 2]. The permanent magnet synchronous motor (PMSM) has been widely employed in such EVs thanks to its features (including high power density, high torque/weight ratio, high efficiency, high torque capability and easy maintenance). It constitutes the best choice for an in-wheel motor [3–5].

The permanent magnet in-wheel motor (PMIWM), installed in a narrow space, is seriously restricted by several uncertainties, such as temperature, magnetic saturation, skin effects, road surface excitation, extra load disturbance, electromagnetic parameter variations and friction force. Each of these factors could lead to distinct degradation of PMIWM performance [6, 7]. Therefore, research on the control strategy for the PMIWM within a complex environment becomes an important step towards improvement of safety, reliability and practicability of the in-wheel motor driven EVs. Speed-tracking accuracy, disturbance rejection and robustness of the PMIWM are the main evaluation indices of such EVs' performance [8, 9].

The PMIWM, however, is a high-order, multivariable and strongly coupled nonlinear system. Decoupling and linearization constitute the keys to controlling the complex nonlinear system. At the same time, the accuracy of the controller is seriously influenced by a variety of uncertainties and nonlinearities of the PMIWM, which makes it difficult to achieve strong robustness and disturbance-rejection performance.

To enhance the robustness and dynamic performance of the PMIWM control system, many efforts have been made [10–13] by researchers around the world to improve control precision. A variety of advanced control techniques have been developed to improve PMIWM performance in the past decades, including direct torque control (DTC), vector control, differential geometry, predictive control, sliding mode control, fuzzy control, support vector machine, model reference adaptive control, inverse system, etc. The DTC is supposed to achieve dynamic decoupling by using torque and flux hysteresis. However, it leads to poor low-speed performance and large torque ripple [14, 15]. The vector control (VC) scheme is an approximate steady-state decoupling approach. The decoupling control of torque and flux could be achieved when flux is accurately observed [16, 17]. The differential geometry (DG) approach is used for the control of nonlinear coupling systems, but it requires an accurate mathematical model [18–20]. Meanwhile, dynamic decoupling and linearization are achieved

*e-mail: liyongthinkpad@outlook.com

Manuscript submitted 2018-01-01, revised 2018-03-05, initially accepted for publication 2018-03-16, published in December 2018.

by using abstract and complex mathematical tools. The model predictive control (MPC) has the ability to explicitly handle constraints. As an optimum control method, the MPC, however, involves a massive computation load and long processing time, mainly suitable for the linear system [21, 22]. The support vector machine (SVM) algorithm is also difficult to implement for large-scale training samples due to its large computation [23–26]. Fuzzy logic control (FLC), unlike others, can obtain better speed tracking performance. The design of fuzzy logic control, however, lacks in systematic methods [27–29]. The membership functions and fuzzy rules are mainly determined by the experts' experience, which is difficult to obtain automatically. The impact of nonlinear factors on the system performance cannot be fundamentally weakened. The sliding mode control (SMC) method is applied to the speed control of a brushless DC motor [30, 32]. SMC improves robustness of the speed control system, but its inherent high-frequency jitter is difficult to eliminate. Meanwhile, the model reference adaptive control (MRAC) technique is mature and easy to implement [33–36]. Adjustment of the adaptive parameters is related to the error and its derivative. The tracking performance of the speed control system is better and more adaptable after introducing the adaptive law, but the MRAC depends on the fixed parameters and the structure of the system. The system will require complex calculations when the system model is uncertain or unknown. The NNC does not depend on the precise mathematical model of the system, but it leads to a slow learning speed, long training time and local minima emerging [37–40]. Reference [6, 10, 41] employed the inverse system method to decouple a bearingless PMSM. However, the PMIWM cannot be completely decoupled by means of a single control method due to the complexity of its system. To effectively decouple the PMIWM system, the hybridization control approach needs to be investigated.

This paper proposes novel internal model control (IMC) for speed control of the PMIWM, which is based on the back-propagation neural network inverse (BPNNI) control scheme. One contribution of this paper is to decouple the PMIWM into a pseudo-linear system using BPNN and inverse system theory. The BPNN is used to obtain a data-driven model of the inverse system. It does not rely on the accurate system model or prior knowledge of the system. The α-order BPNNI system is easy to implement according to the system relative orders and based on correct training of neural networks. The other contribution of this paper is to overcome unpredicted disturbances and improve the robustness and dynamic performance of the PMIWM by means of the IMC control scheme. The proposed BPNNI-IMC scheme combines the advantages of control methods, resulting in prompt response, high accuracy and tangible decoupling effectiveness of the control method.

The paper is organized as follows: first, in Section 2, PMIWM modeling and invertibility analysis are sought. In Section 3, the BPNNI control scheme is described. After that, the IMC method is presented in detail in Section 4. Simulation and experimental works are presented and discussed in Section 5. Section 6 is devoted to the conclusions of the present work as well as prospects for future research.

2. Inverse system modeling

2.1. Mathematical model of the PMIWM. Figure 1 illustrates the cross-sectional view of the out-rotor PMIWM. The concentrated armature coil is the element wound around each stator pole. Permanent magnets are sandwiched between the rotor and the stator to adjust to the airgap flux. The stator of the motor adopts three-phase winding with fractional slots per pole per phase, thus offering the low cogging torque highly desirable for application in vehicles [42].

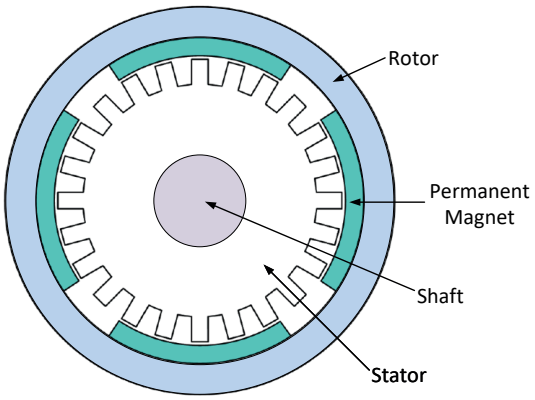

Fig. 1. Block diagram of the PMIWM

The mathematical model of the PMIWM in the synchronously rotating d–q reference frame is expressed as Eq. (1):

$$\begin{cases} \dfrac{di_d}{dt} = \dfrac{1}{L}\left(u_d - R_s i_d + L i_q \omega\right) \\ \dfrac{di_q}{dt} = \dfrac{1}{L}\left(u_q - R_s i_q + L i_d \omega - \psi_f \omega\right) \end{cases} \tag{1}$$

where i_d and i_q are the d-axis and q-axis currents of the stator, respectively. u_d and u_q represent the voltage component on the d-axis and q-axis, respectively. ω denotes the electrical angular velocity of the PMIWM rotor. L indicates the inductance of the d-axis and q-axis, respectively. R_s shows the stator resistance and ψ_f stands for permanent magnet flux linkage of the rotor.

The electromagnetic torque equation of the PMIWM in the d–q coordinate is described as Eq. (2):

$$T_e = \frac{3}{2} p_n \psi_f i_q \tag{2}$$

where p_n is the number of pole pairs.

The motion equation of the PMIWM is shown as:

$$J_M \frac{d}{dt}\left(\frac{\omega}{p_n}\right) = T_e - T_L - B\frac{\omega}{p_n} \tag{3}$$

where J_M denotes the moment inertia of the PMIWM. T_L is the load torque and B is the coefficient of motion damping, which is in fact ignored.

Thus, according to Eq. (2) and Eq. (3), the motion equation could be re-written as:

$$\frac{d\omega}{dt} = \frac{3}{2}\frac{p_n^2}{J_M}\psi_f i_q - \frac{T_L p_n}{J_M}. \tag{4}$$

2.2. Invertibility analysis of the PMIWM. In this paper, rotor flux oriented vector control is applied to the PMIWM. Rotor speed and flux can be dynamically decoupling-controlled using the inverse system method. Therefore, reversibility of the mathematical model of the PMIWM should be discussed first.

The control purpose is to decouple speed ω, d axis current i_d, q axis current i_q and flux ψ_f. Thus, i_d and ω are selected as outputs of the PMIWM, whose variables are $y = [y_1, y_2]^T = [i_d, \omega]^T$. Furthermore, u_d and u_q are selected as control variables, where $u = [u_1, u_2]^T = [u_d, u_q]^T$, while i_d, i_q and ω are state variables, where $x = [x_1, x_2, x_3]^T = [i_d, i_q, \omega]^T$. Consequently, the corresponding state equation of the nonlinear system can be formulated as:

$$\dot{x} = f(x,u) = \begin{bmatrix} \dot{x}_1 \\ \dot{x}_2 \\ \dot{x}_3 \end{bmatrix} = \begin{bmatrix} \frac{1}{L}\left(u_1 - R_s x_1 + L x_2 x_3\right) \\ \frac{1}{L}\left(u_2 - R_s i_2 + L x_1 x_3 - \psi_f x_3\right) \\ \frac{3}{2}\frac{p_n^2 \psi_f x_2}{J_M} - \frac{p_n T_L}{J_M} \end{bmatrix}. \tag{5}$$

According to the inverse system theory, the Jacobian matrix of the output derivation can be expressed as:

$$A(x,u) = \begin{bmatrix} \frac{\partial \dot{y}_1}{\partial u_1} & \frac{\partial \dot{y}_1}{\partial u_2} \\ \frac{\partial \ddot{y}_2}{\partial u_1} & \frac{\partial \ddot{y}_2}{\partial u_2} \end{bmatrix} = \begin{bmatrix} \frac{1}{L} & 0 \\ 0 & \frac{3}{2J_M L} p_n^2 \psi_f \end{bmatrix}. \tag{6}$$

Flux ψ_f of the PMWIM could not be zero if $A(x,u)$ were to be a nonsingular matrix. The relative order of the system is $\alpha = (\alpha_1, \alpha_2) = (1, 2)$, and $\alpha_1 + \alpha_2 = 3$. As a result of $\sum_{i=1}^{2} \alpha_1 = 3 \leq n$, n is the number of the state variable, which satisfies the sufficient conditions of the existence of the inverse system [2, 23]. Thus, in accordance with the inverse system theory, it can be concluded that there exists the α-order inverse system of the original system. The inverse system of the PMIWM can be expressed as:

$$u = (u_1, u_2) = \xi\left(y_1, \dot{y}_1, y_2, \dot{y}_2, \ddot{y}_2, [v_1, v_2]^T\right) \tag{7}$$

where v_1 and v_2 are the new input vectors.

3. RBFNNI-based decoupling scheme of the PMIWM

However, as aforementioned, it is difficult to completely decouple the PMIWM, even if its inverse system has been expressed in the above section. Furthermore, the unpredictable disturbance and parameter perturbation during the operation of the PMIWM could have a massive influence on the motor's performance. Thus the BPNNI , is introduced in this section to improve PMIWM robustness.

3.1. Back-propagation neural network. Although there are many neural network models, the model mainly used in the area of pattern recognition or classification is the feedforward/backpropagation (BP) network [43, 44]. The BP, originally introduced by Werbos in 1974, owes much of its development to Rumelhart. The BP neural network (BPNN) consists of fully interconnected rows of processing units called nodes, which are organized into groups named layers. Internal layers provide the interconnections between the input and output. The BPNN is fitted by means of training the network with known input/output data sets, sometimes referred to as facts. The training paradigm finds a set of weight values that minimizes the error across the set of facts. During the training, differences between actual outputs and predicted outputs are propagated back through the architectural structure of the network. The importance of this process is that, as the network is trained, the neurons in the intermediate layers organize themselves in such a way that different neurons learn to recognize different characteristics of the total input space. Moreover, in order to improve the adaptive ability and parameter change rejection of the control system, the Takagi-Sugeno fuzzy inference system is introduced into the BPNN.

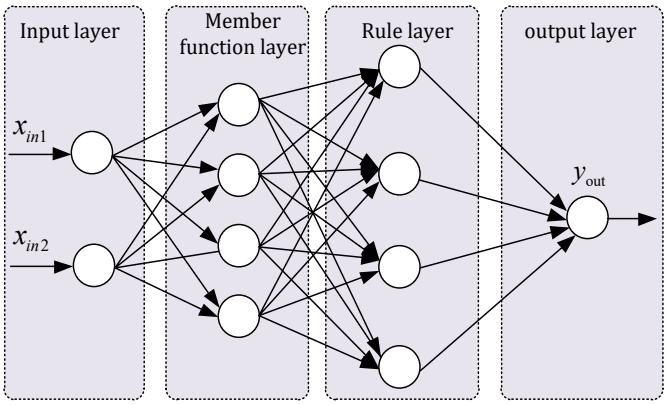

Fig. 2. BPNN chart

The BPNN shown in Fig. 2 consists of 4 layers: input layer, membership function layer, rule layer and output layer. The parameters of the BPNN, including layer numbers, the neuron number in each layer, weight coefficient and learning rate, can be optimized by trial and error [45]. As illustrated in Fig. 2, the first layer is the input layer, which contains two neurons. The input variable is represented by x_1 and x_2. The second layer is the function layer, which renders the output of the first layer fuzzified. The third layer is the fuzzy law layer, which will generate fuzzy inference. The fourth layer is the output layer, which is represented by y_{out}.

Variables x_1 and x_2 are supposed to be introduced into the input layer, which contains 2 neurons. The input and output of the 2 neurons are expressed as:

$$\begin{cases} net_i^1(M) = x_i^1(M) \\ y_i^1(M) = f_i^1\left(net_i^1(M)\right) = net_i^1(M) \end{cases} \tag{8}$$

where $i = 1, 2$; M stands for the iterations, $x_1^1(M) = \omega_s(M)$, $x_2^1(M) = \omega(M)$; and *net* is the neural network.

The membership function layer is used to fuzzify y_1^1 and y_2^1. The membership function during the fuzzy process is the Gaussian function. Each neuron in the membership function layer has functional ability. The input and output of node j could be expressed as:

$$\begin{cases} net_j^2(M) = \dfrac{\left(x_j^2 - m_j\right)^2}{\sigma_j^2} \\ y_j^2(M) = f_j^2\left(net_j^2(M)\right) = esp\left(net_j^2(M)\right) \end{cases} \quad \text{and } j = 1, \cdots, n \tag{9}$$

where x_j^2 is the input of the *j-th* neuron, m_j is the average value and standard deviation of the *j-th* membership function, and n is the total number of input variables, equal to the total number of neurons in the membership function layer.

The error equation of the membership function layer is described as:

$$\delta_j^2(M) = -\frac{\partial E_I(M)}{\partial net_j^2(M)} = \sum_k \delta_k^3(M) y_k^3(M). \tag{10}$$

The rule layer is employed to complete fuzzy inference work. The input and output of the *k-th* neuron are written as:

$$\begin{cases} net_k^3(M) = \prod_j w_{jk}^3 x_j^3(M) \\ y_k^3(M) = f_k^3\left(net_k^3(M)\right) = net_k^3(M) \end{cases} \tag{11}$$

where $x_j^3(N)$ is the input of the *k-th* neuron, and w_{jk}^3 is the corresponding weight coefficient of $x_j^3(N)$.

The error in the rule layer should be calculated during the training process, and the equations are written as:

$$\delta_k^3(M) = -\frac{\partial E_I(M)}{\partial net_k^3(M)} = \delta_o^4(M) x_k^4(M). \tag{12}$$

There is only one neuron Σ in the output layer. The input and output of Σ are shown by:

$$\begin{cases} net_o^4(M) = \sum_{k=1}^{R_1} w_k^4 x_k^4(M) \\ y_o^4(M) = f_o^4\left(net_o^4(M)\right) = net_o^4(M) \end{cases} \tag{13}$$

where $x_k^4(M)$ is the input of neuron Σ, w_k^4 is the corresponding weight coefficient of $x_k^4(M)$ and R_1 is the total number of fuzzy rules.

To satisfy the actual operation of the PMIWM, the BPNN requires continuous on-line training. Training a network begins by randomly assigning weighting factors for each node interconnection and a bias term. The learning rate is an adjustable factor that controls the speed of the learning process. Generally, network learning can be facilitated by starting at a high learning rate. Speed learning reduces the probability that the network solution will settle into a non-optimum and local error minimum.

The property standard function is defined as:

$$E_1(M) = \frac{\left(\omega(M) - \omega^*(M)\right)^2}{2}. \tag{14}$$

According to the BP algorithm, the error of the output layer could be described as:

$$\begin{aligned} \delta_o^4(M) &= -\frac{\partial E_I(M)}{\partial net_o^4(M)} = \\ &= -\left[\frac{\partial E_I(M)\partial e_i(M)\partial \omega_r^*(M) y_o^4(M)}{\partial e_i(M)\partial \omega_r^*(M) y_o^4(M) net_o^4(M)}\right]. \end{aligned} \tag{15}$$

3.2. BPNNI system construction. To take the advantages of the BPNN control method and of the inverse control approach, two schemes are combined to establish a novel decoupling control system. BPNN is employed to realize the reversibility of the PMIWM control system. By cascading certain integrators on the left side of the BPNN block, a novel NNI control system is established with the ability of generalization. It will improve robustness and fault-tolerant performance. The proposed NNI is located on the left side of the PMIWM shown in Fig. 3, which leads to emergence of a pseudo-linear system for system decoupling. The NNI control approach does not require an accurate mathematical model of the PMIWM, yet it improves robustness and the ability to reject disturbances.

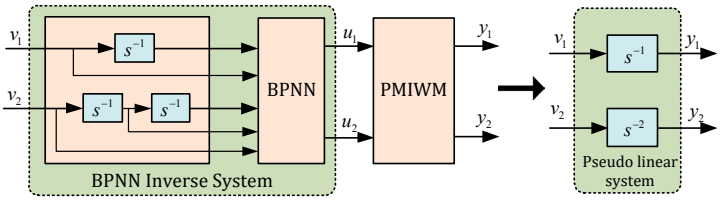

Fig. 3. Pseudo-linear system

The simple drive cycle is used as the reference speed in the neural network training process. Three sets of data, selected from the drive cycle, are shown in Table 1 in the rapidly changing area. The data are employed as the training sample

of the BPNN. The input samples that go into the network work periodically during the whole training process. The output error does not enter the permitted range before convergence of the neural network. The learning rate is set at 0.08 during the training process. The BP neural network is supposed to meet the requirement when the training error is less than 0.01 after 600 epochs of training. The BPNN is established and ready for the PMIWM control system.

Table 1
Training samples of BPNN

Number	Team 1	Team 2	Team 3
1	301.99	697.95	684.53
2	335.55	644.26	644.26
3	369.10	590.57	603.99
4	402.66	536.88	563.73
5	436.22	536.88	523.46
6	469.77	536.88	483.19
7	503.33	536.88	442.93
8	570.44	536.88	362.39
9	637.55	429.50	281.86
10	671.10	375.82	241.59

4. BPNNI-based IMC design

The IMC scheme was introduced by Garcia and Morari and then subjected to intensive research during the past decades. The IMC is effective at tracking, rejecting disturbance and enhancing robustness. The IMC method was originally employed to process a control system and then extended to the motor control system, which relies on the "internal model" principle, including a model of the plant [46, 47]. It should be pointed out that the conventional IMC method could provide an adequate suppressing ability for the disturbances added to the output channel. However, it might not provide a satisfactory load disturbance rejection property for the disturbances added to the input channel when the process dynamics are much slower than the desired closed loop dynamics [48–50]. Figure 4 shows the structure of the 2-DOF internal model controller of the PMIWM.

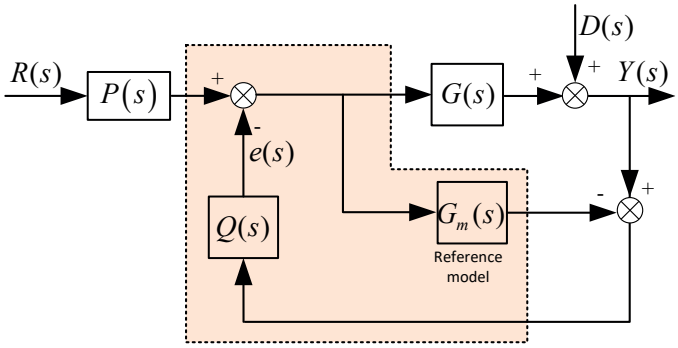

Fig. 4. Control diagram of 2-DOF IMC

where $G(s)$ is the controlled object, and $G_m(s)$ the ideal internal model. $Q(s)$ and $P(s)$ are the internal model controllers. $Y(s)$ is the output of the system. $D(s)$ stands for external disturbance. $R(s)$ is the input of the system.

The PMIWM output is expressed as:

$$Y(s) = G_m(s)P(s)R(s) + \big(1 - Q(s)G_m(s)\big)D(s). \quad (16)$$

Equation (17) illustrates that tracking performance is determined by $P(s)$, and disturbance rejection relies on $Q(s)$. To track the input $R(s)$ without any steady-state error and to improve robustness, low pass filters $F_1(s)$ and $F_2(s)$ are introduced into the internal model controllers $G_{c1}(s)$ and $G_{c2}(s)$, which could be expressed as:

$$\begin{cases} P(s) = F_1(s)G_m^{-1}(s) \\ Q(s) = F_2(s)G_m^{-1}(s). \end{cases} \quad (17)$$

Low pass filters $F_1(s)$ and $F_2(s)$ are commonly described as follows:

$$\begin{cases} F_1(s) = \dfrac{1}{(\lambda_1 s + 1)^2} \\ F_2(s) = \dfrac{1}{(\lambda_2 s + 1)^2} \end{cases} \quad (18)$$

where λ_1 and λ_2 are the time constants of the filter.

Figure 5 is a structure equivalent to Fig. 4.

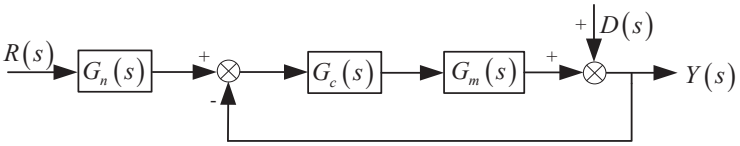

Fig. 5. Diagram of the 2-DOF internal model controller

The output error equation of the closed-loop system is represented by:

$$E(s) = R(s)G_n(s) - Y(s) = \\ = \frac{[1 + G_c(s)G_m(s) - G_n(s)G_c(s)G_m(s)]R(s) - D(s)}{1 + G_c(s)G_m(s)}. \quad (19)$$

As for the step signals, if $R(s) = \frac{R_0}{s}$, the steady state error could be given as:

$$E(\infty) = \lim_{s\to 0} s\left(\frac{(\lambda_1 s + 1)^2 - 1}{(\lambda_1 s + 1)^2}\frac{R_0}{s}\right) = 0. \quad (20)$$

As for the sinusoidal signal, and if $R(s) = \frac{R_0}{s^2}$, the steady state error could be written as:

$$E(\infty) = \lim_{s\to 0} s\left(\frac{(\lambda_1 s+1)^2 - 1}{(\lambda_1 s+1)^2}\,\frac{R_0}{s^2}\right) = 0. \tag{21}$$

Hence, the closed-loop control system of the PMIWM could track the step and sinusoidal signal without any obvious steady state errors.

The overall control scheme of the PMIWM is shown in Fig. 6.

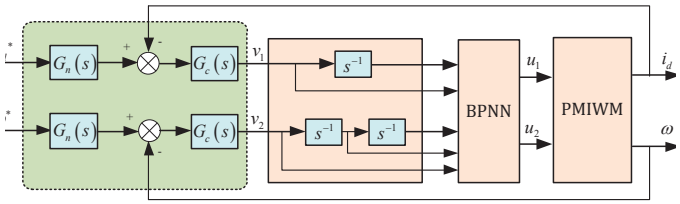

Fig. 6. Overall BPNNI-based IMC diagram

5. Simulation and experimental validation

To validate the effectiveness and performance of the proposed BPNNI-based IMC control scheme of the PMIWM, simulation and experiments have been developed. Comparative results of the BPNNI control scheme are measured. IMC parameters λ_1 and λ_2 are 0.4 and 0.8, respectively. The current loops bandwidth is designed to be 5 times that of traditional current loops. IGBT is used as the bi-directional converter. The higher the frequency, the larger the loss. According to the Shannon's sampling theorem, the upper limit switching frequency of the converter is half of the carrier frequency. $i_d = 0$ is used for vector control of the PMIWM.

5.1. Simulation verification. Comparative studies of the PMIWM control system are carried out with the use of Matlab/Simulink software. The control system is modeled in Simulink. The nominal power of the PMIWM motor is 8 kW. Nominal speed is 1600 r/min and nominal torque is 100 Nm.

1) Decoupling and tracking property

To test decoupling and tracking property of the control system, motor speed ω is set to increase from 0 r/min to 1200 r/min. The simulation results from the motor with BPNNI control and the proposed BPNNI-based IMC control are illustrated in Fig. 7, from the top to the bottom, respectively.

Figure 7 illustrates that the BPNNI-based control strategy visibly reduces the fluctuations as compared with the BPNNI control scheme. This proves that the proposed BPNNI-based IMC approach will not only guarantee stability of the PMIWM control system, but also effectively solve the strong coupling problems. Far more importantly, it obviously has excellent properties with only slight overshoot and smaller oscillation once the system reaches the steady state.

From Fig. 7 it can be seen that the motor speed manifests either small or large fluctuations at $t = 0.01$ s. The fluctuations last for a short time, from $t = 0.01$ s. After that, the speed goes to a steady-state value, which is 1200 r/min. It thus takes less than 0.02 s from the start to stabilized time with both control schemes. The simulation error with different control schemes is less than 80 r/min before getting to stabilized time. After 0.02 s, fluctuations with the BPNNI control method are larger than that those with the proposed control approach, which could be seen from the simulation error speed at the bottom in Fig. 7.

To further test decoupling and tracking performance of the PMIWM control system, a simple drive cycle is selected as the speed reference. The reference speed steps up from 100 r/min to 300 r/min, and then decreases to 200 r/min. To compare the performance of the two control methods, the output speed responses of the PMIWM measured with the two controllers are compared and shown in Fig. 8.

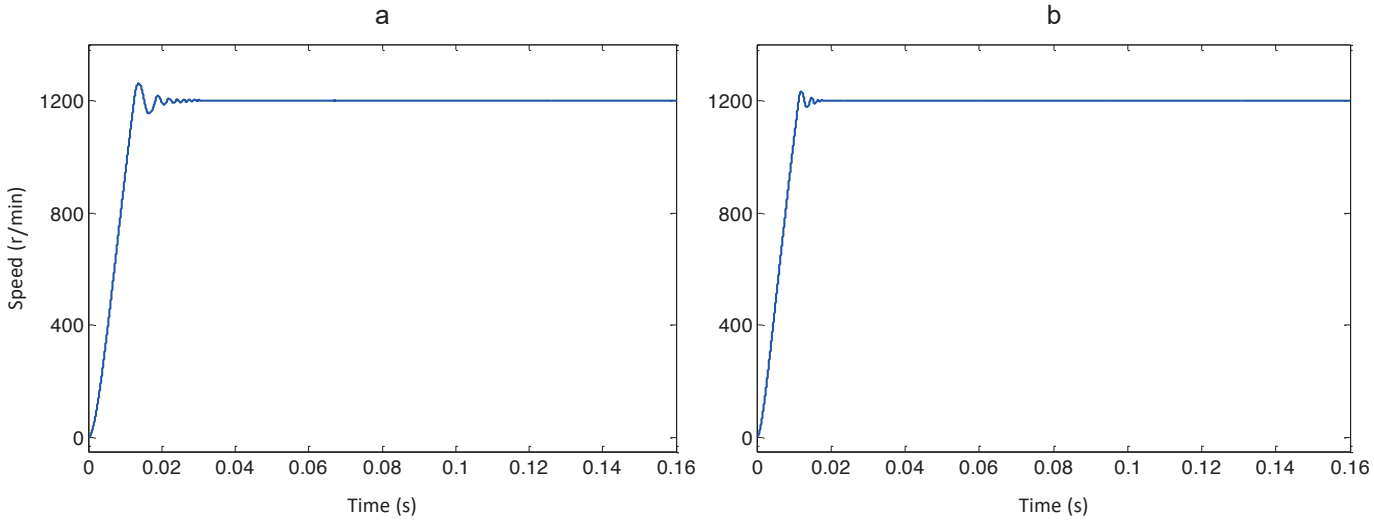

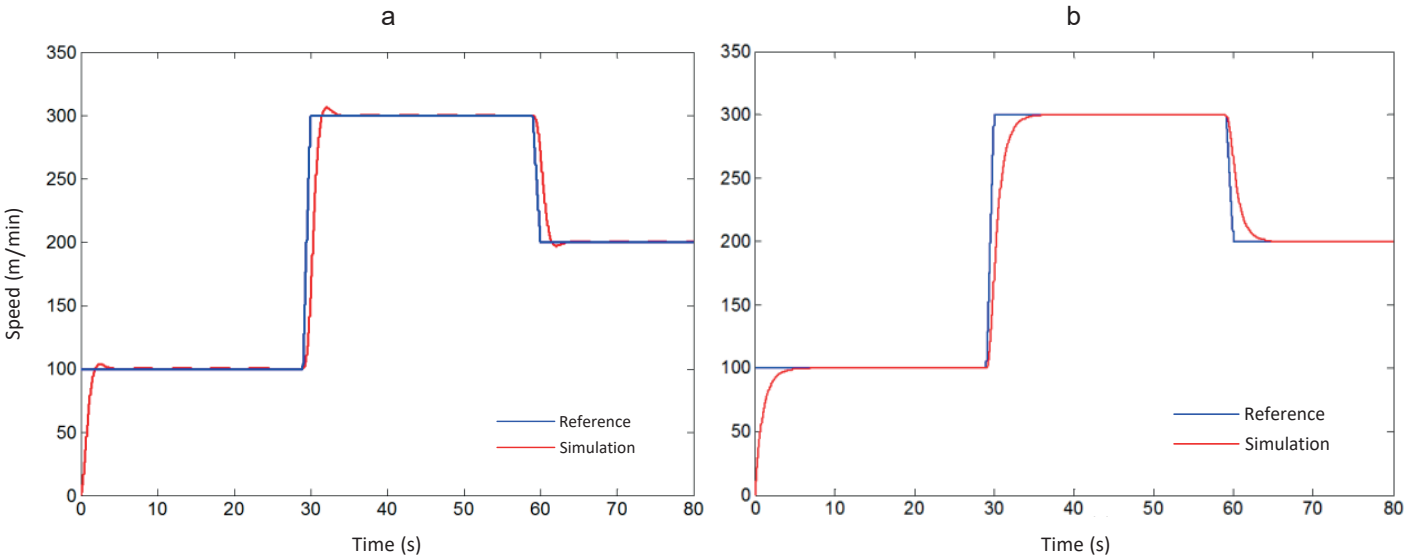

Fig. 8. Simulation results of decoupling and tracking property with different control schemes: a) BPNNI control, b) proposed control

It can be obviously seen that the proposed control scheme reduces the overshoot and shortens the transient time. Figure 8a demonstrates that the overshoot is 2.92% at 30 s, with a 2.18 s settling time. Then it is 2.88% at 60 s, with a 2.06 s settling time. Compared with Fig. 8a, the speed tracks the reference very well in Fig. 8b, and there is no obvious steady-state error. And the settling times are 1.82 s and 1.77 s in Fig. 8b, respectively.

2) Disturbance rejection and robustness performance

In order to verify the disturbance rejection and robustness performance of the proposed control scheme under a sudden load impact, simulation tests have been performed with the exerted load shown in Fig. 9. The motor operates at a constant speed of 1200 r/min. A 6 Nm load is added to the motor at 0.1 s, which lasts for 0.1 s. Then the load is decreased from 6 Nm to 3 Nm at 0.2 s.

From top to bottom, simulation results of the speed trajectory, close-up at 0.1 s and close-up at 0.2 s, are shown in Fig. 10, respectively. Obviously, Fig. 10 shows that there are some speed fluctuations under the BPNNI control at $t = 0.1$ s and $t = 0.2$ s, when the loads are applied. As is seen in Fig. 10, the close-ups illustrate that the speed response has a large overshoot of 1.27% at 0.1 s and 1.43% at 0.2 s, respectively. It could be noted that in Fig. 10 the settling time is 0.01 s from 0.1 s and 0.011 s from 0.2 s, respectively.

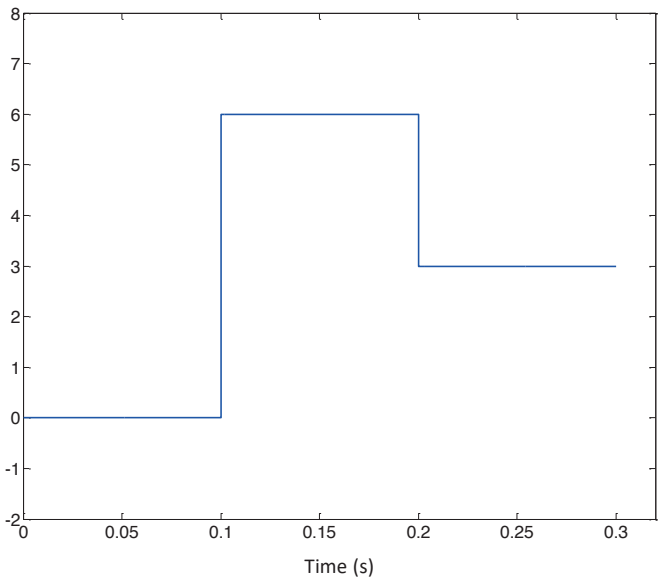

Fig. 9. Simulation results of sudden load disturbance

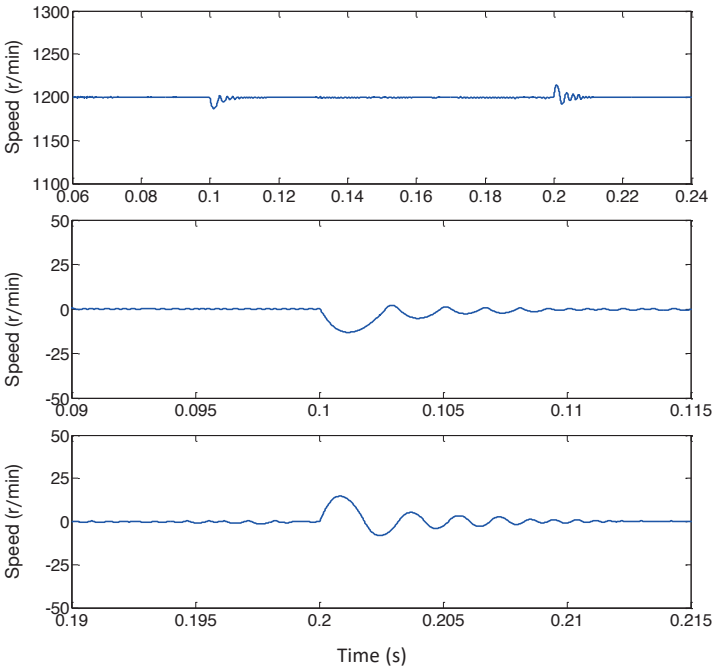

Fig. 10. Simulation results of sudden load disturbance with BPNNI control

The speed responses from the proposed control system are shown in Fig. 11, from top to bottom. Simulation results of the speed trajectory, close-up at 0.1 s and close-up at 0.2 s, are also respectively illustrated. Compared to Fig. 10, no noticeable fluctuations exist at $t = 0.1$ s and $t = 0.2$ s. The close-ups of speed trajectory at $t = 0.1$ s and $t = 0.2$ s are shown in Fig. 11. The speed response has a small overshoot of 0.47% at 0.1 s and 0.56% at 0.2 s, respectively. The settling time as shown in Fig. 11 is 0.009 s from 0.1 s and 0.0104 s from 0.2 s, respectively.

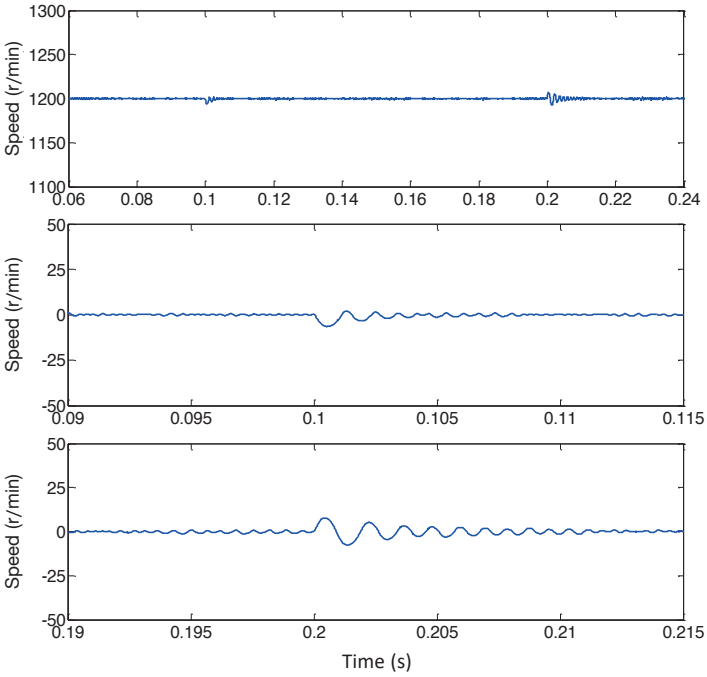

Fig. 11. Simulation results of sudden load disturbance with the proposed control scheme

5.2. Experimental verification. Matlab and dSPACE software provide a rapid prototyping environment for testing and deploying real-time systems. The control scheme is established in Simulink, which can create an executable code for the host PC. The executable code is downloaded to a target PC, in which the proposed control approach is implemented. Namely, the control scheme can be tested in a "soft motor controller". A dSPACE-based hardware-in-the-loop (HIL) test bench is built in the lab, which consists of a user PC, dSPACE hardware, a control box and a control console. The I/O boards, A/D boards, D/A boards and Encoder boards are all allowed to be programmed for the aforementioned models using Simulink blocks. Then, the executable code will be created and downloaded from the user PC to the dSPACE hardware. Communication among the user PC, the hardware boards inside the control box and dSPACE hardware is realized via the RS 232/485 interface. The I/O board converts signals read by the physical sensor into the EV model in the Simulink program. The A/D board transforms an analog signal into a digital signal, which can be read by the user PC. The control desk software is the experiment and test environment, which is used for parameter adjusting, wave observing

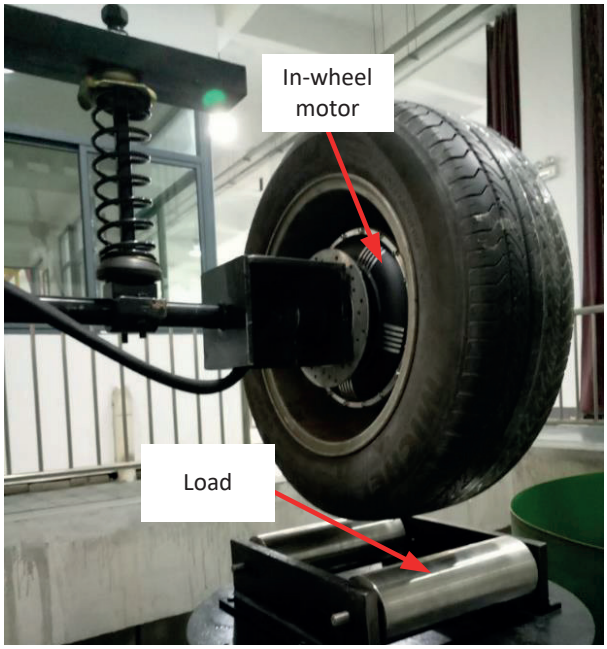

Fig. 12. dSPACE-based HIL test bench

and data recording. The Encoder board is used to convert the speed signal of the PMIWM. The PMIWM is installed inside the wheel hub. The dSPACE-based HIL test bench is presented in Fig. 12.

1) Decoupling and tracking property

To evaluate decoupling and tracking properties of the proposed BPNNI-based IMC scheme, decoupling and tracking experiments of the PMIWM are carried out on the above-mentioned HIL test bench. After choosing the appropriate incentive signals, the corresponding responses of motor speed ω could be obtained under various conditions. The decoupling effectiveness of the proposed BPNNI-based IMC scheme could be emulated by q-axis current i_q and motor speed ω. The control system of the PMIWM is set to increase from 0 rpm to 1200 r/min. A BPNNI control scheme is also carried out for comparison. Decoupling and tracking properties of BPNNI control and the proposed BPNNI-based IMC control scheme are shown in Fig. 13, which presents, from top to bottom: output speed with the BPNNI control scheme, the BPNNI-based IMC control approach and comparison between the output speeds, respectively.

As shown clearly by Fig. 13, fluctuations in the proposed BPNNI-based IMC control are smaller than those within the BPNNI control scheme. Moreover, the speed trajectory of the proposed control method is more stable than that of the BPNNI control approach. The actual responses illustrate that parameters and variables in the speed regulator decouple better with the proposed control scheme than with the BPNNI control method. It can be seen that the experimental results actually agree with the simulation results.

To further compare decoupling and tracking performance, experiments with two different control schemes were carried

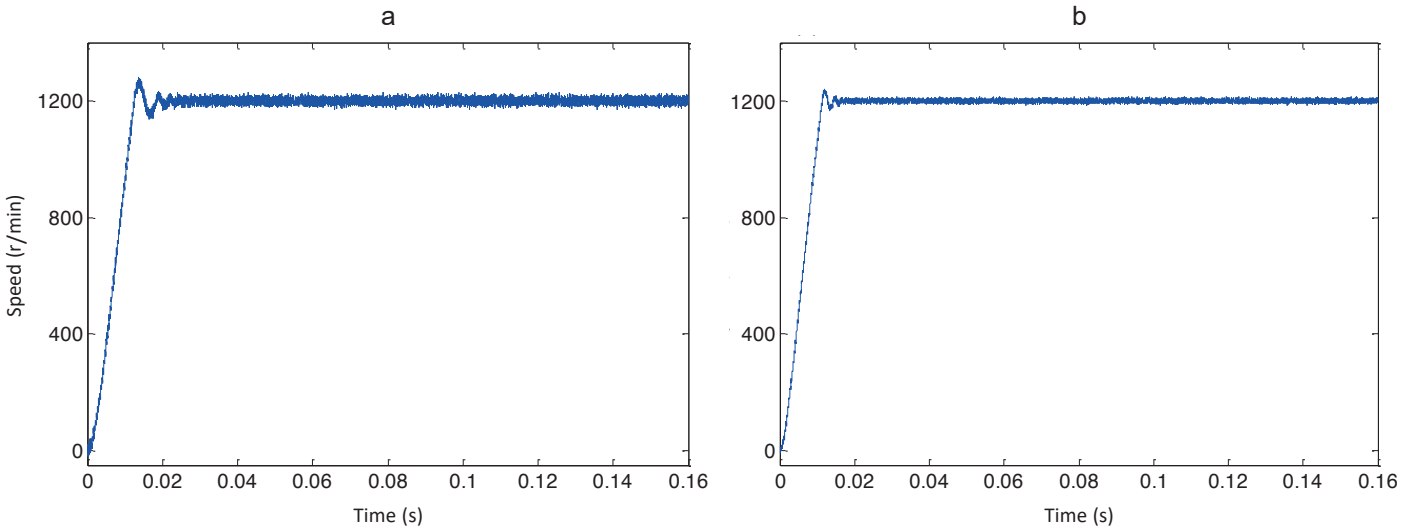

Fig. 13. Experimental results of decoupling and tracking properties within different control schemes: a) BPNNI control, b) proposed control

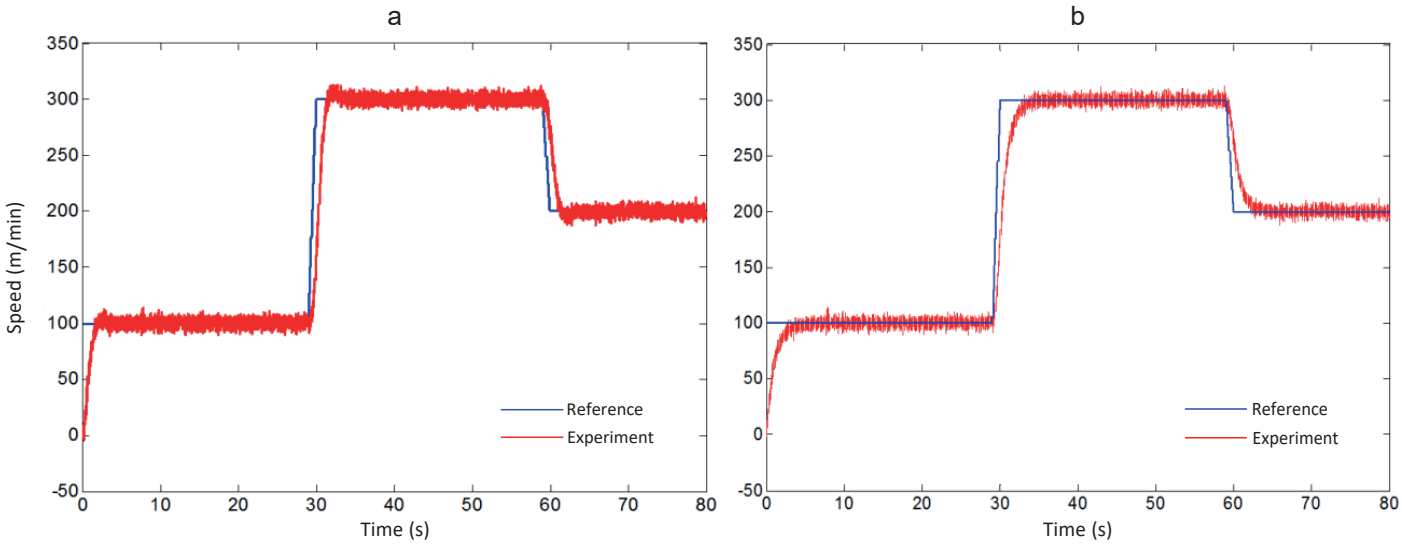

Fig. 14. Experimental results of decoupling and tracking properties within different control schemes: a) BPNNI control, b) proposed control

out on the test bench. The experimental results, as shown in Fig. 14, comply with the simulation results.

As shown in Fig. 14a, speed under the BPNNI controller tracks the reference closely, even though the actual speed oscillates. The overshoots are 2.97% at 30 s and 2.95% at 60 s under BPNNI control, respectively. The response in Fig. 14(b) is much slower than that in Fig. 14a. The curve in Fig. 14b shows overshoots at 0.01% at 30 s and 0.02% at 60 s under the proposed control scheme, respectively. Figure 14b illustrates that the proposed controller performs well as far as both response time and smooth overshoot are concerned. Moreover, the speed trajectory under the proposed control scheme is more stable than for the BPNNI control.

2) Disturbance rejection and robustness performance

In this section, experiments are carried out to verify the performance of disturbance rejection and robustness with a sudden load impact on the control system. The curve of the load disturbance employed in the experiment is shown in Fig. 15.

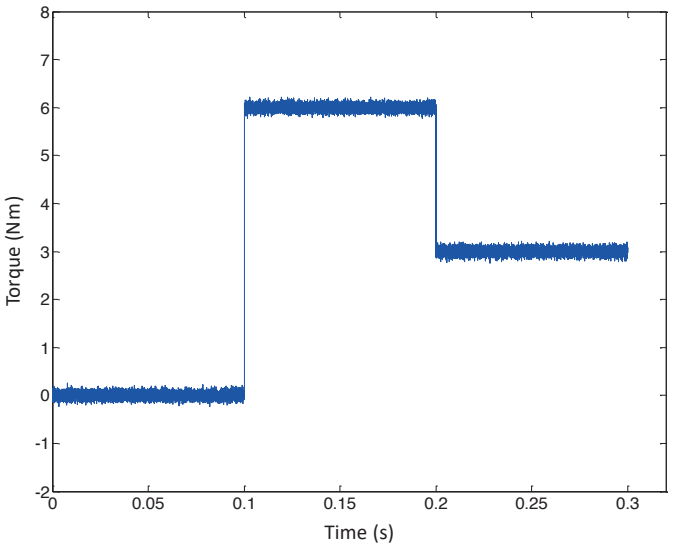

Fig. 15. Experimental results of sudden load disturbance

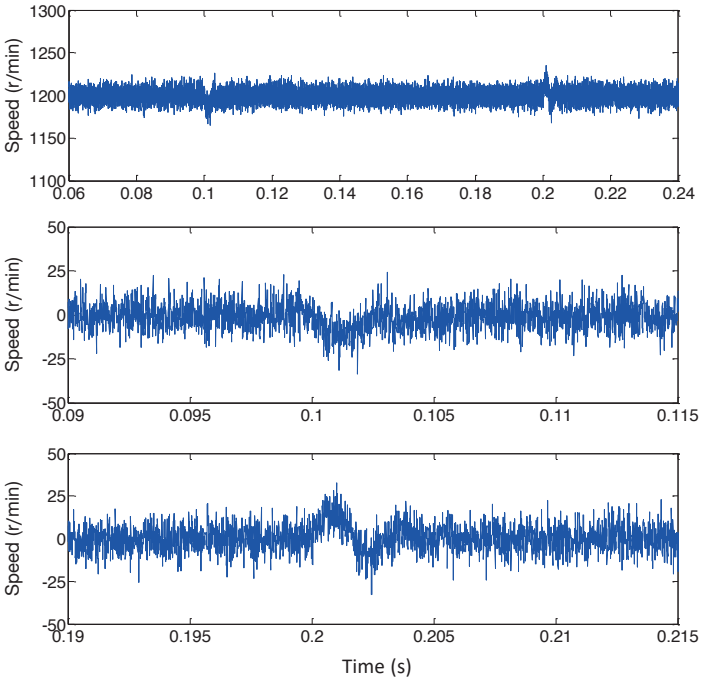

Fig. 16. Experimental results of sudden load disturbance with BPNNI control

The experimental results of disturbance rejection with BPNNI control and the proposed control are shown in Fig. 16 and Fig. 17, respectively. The output speed trajectories, close-up at 0.1 s and close-up at 0.2 s, are shown in Fig. 16, from top to bottom, respectively. Obviously, as seen in Fig. 16, the close-ups illustrate that the speed response has a large overshoot of 1.29% at 0.1 s and 1.46% at 0.2 s, respectively. The speed responses from the proposed control system are shown in Fig. 17, in which the speed trajectories, close-up at 0.1 s and close-up at 0.2 s, are illustrated, from top to bottom, respectively. From Fig. 17, we can see that the speed response has a small overshoot of 0.50% at 0.1 s and 0.61% at 0.2 s, respectively.

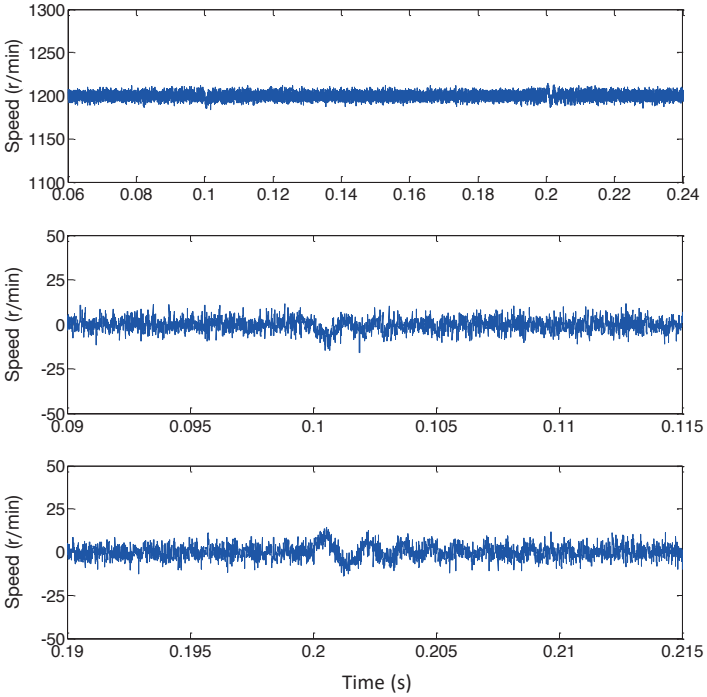

Fig. 17. Experimental results of sudden load disturbance with the proposed control

Obviously, from Table 2 we can see that compared with the other two control strategies, the proposed BPNNI-based IMC scheme has prominent advantages in the form of the decoupling effect, trajectory tracking, disturbance rejection and robustness. Furthermore, to compare the properties of the different control schemes, the comparisons of experimental results are given to verify the effectiveness of the proposed control scheme illustrated quantitatively in Table 2.

Table 2.
Experimental comparisons of tracking, disturbance rejection and robustness with different control approaches

Control strategy	Decoupling and tracking (simple drive cycle)			Disturbance rejection (constant reference speed)		
	Over-Shoot (%)	Settling time (s)	Step time (s)	Over-shoot (%)	Settling time (s)	Step time (s)
BPNNI control	2.97	2.43	30	1.29	0.011	0.1
	2.95	2.39	60	1.46	0.013	0.2
Proposed control scheme	0.01	1.96	30	0.50	0.010	0.1
	0.02	1.89	60	0.61	0.005	0.2

6. Conclusions

This paper presents a novel BPNNI-based IMC scheme for the PMIWM that guarantees tracking performance, disturbance rejection and system robustness in case of parameter uncertainties and load disturbances. Based on the back-propagation BPNNI controller, the proposed control scheme employs a 2-DOF internal model controller (IMC) that acts as an extra feedback controller for the newly developed pseudo-linear system. Results of comparative simulation and real-time HIL experiments demonstrate that: first, the PMIWM drive system could be effectively decoupled with the proposed control scheme, where the nonlinear system was transformed into a pseudo-linear system. Then, by introducing the IMC scheme into the pseudo-linear system, the whole system becomes characterized by a solid dynamic, disturbance rejection and robustness. Last but not least, the proposed control scheme is superior to the BPNNI control approach in tracking precision, robustness and stability under various conditions of the PMIWM control system. To recapitulate, this paper, inspired by the concept of deep learning, is expected to overcome the disadvantages of traditional NN control for the PMIWM. However, despite the efforts made regarding the NN control

method in this paper, questions concerning the layer number and neurons in each layer remain to be discussed in future studies.

Acknowledgements. This project is supported by the National Natural Science Foundation of China (51705213, U1664258), the Primary Research & Development Plan of Jiangsu Province (BE2017129), the Natural Science Foundation of Jiangsu Province (BK20160525).

References

[1] X. Sun, L. Chen, H. Jiang, and Z. Yang, "High-performance control for a bearingless permanent magnet synchronous motor using neural network inverse scheme plus internal model controllers", *IEEE Transactions on Industrial Electronics* 63(6), 3479–3488 (2016).

[2] Y. Li, B. Li, X. Xu, and X. Sun, "A nonlinear decoupling approach using RBFNNI-based robust pole placement for a permanent magnet in-wheel motor", *IEEE Access* 6, 1844–1854 (2018).

[3] R. He and Y. Xu, "Shift schedule of parallel hybrid electric vehicles under hybrid driving mode", *Journal of Jiangsu University (Natural Science Edition)* 37(6), 657–662 (2016).

[4] S. Lyshevski, "Control of high-precision direct-drive mechatronic servos: Tracking control with adaptive friction estimation and compensation", *Mechatronics* 43, 1–5 (2017).

[5] C. Pan, L. Zhang, L. Chen, H. Jiang, and Y. Ding, "Heating analysis and experiment of lithium battery for different discharge rates", *Journal of Jiangsu University (Natural Science Edition)* 38(2), 133–138 (2017).

[6] X. Sun, B. Su, L. Chen, Z. Yang, and K. Li, "Design and analysis of interior composite-rotor bearingless permanent magnet synchronous motors with two layer permanent magnets", *Bull. Pol. Ac.: Tech*. 65(6), 833–843 (2017).

[7] B. Li, A. Goodarzi, A. Khajepour, S. Chen, and B. Litkouhi, "An optimal torque distribution control strategy for four-independent wheel drive electric vehicles", *Vehicle System Dynamics* 53(8), 1172–1189 (2015).

[8] X. Sun, Z. Xue, S, Han, L. Chen, X. Xu, and Z. Yang, "Comparative study of fault-tolerant performance of a segmented rotor SRM and a conventional SRM", *Bull. Pol. Ac.: Tech*. 65(3), 375–381 (2017).

[9] N. Zhang, C. Zhou, Z. Gao, and Y. Li, "Torque distribution strategy of PHEV based on FCMAC neural network", *Journal of Jiangsu University (Natural Science Edition)* 38(6), 652–657, (2017)

[10] X. Sun, B. Su, L. Chen, Z. Yang, X. Xu, and Z. Shi, "Precise control of a four degree-of-freedom permanent magnet biased active magnetic bearing system in a magnetically suspended direct-driven spindle using neural network inverse scheme" *Mechanical Systems and Signal Processing* 88, 36–48 (2017).

[11] K. Urbanski, "A new sensorless speed control structure for PMSM using reference model", *Bull. Pol. Ac.: Tech.* 65(4), 489–496 (2017).

[12] L. Wang, "Automatic tuning of PID controllers using frequency sampling filters", *IET Control Theory & Applications* 15(5), 835–842 (2017).

[13] J. Zhou, Q. Deng, and C. Kang, "Regular expression matching algorithm based on parameters setting", *Journal of Jiangsu University (Natural Science Edition* 37(2), 194–200 (2016).

[14] A. Ammar, A. Bourek, and A. Benakcha, "Nonlinear SVM-DTC for induction motor drive using input-output feedback linearization and high order sliding mode control", *ISA Transactions* 67, 428–442 (2017).

[15] A. Khedher, and M. Mimouni, "Sensorless-adaptive DTC of double star induction motor original", *Energy Conversion and Management* 51(12), 2878–2892 (2010).

[16] M. Janaszek, "Structures of vector control of n-phase motor drives based on generalized Clarke transformation", *Bull. Pol. Ac.: Tech.* 64 (4), 865–872 (2016).

[17] Q. Song, H. Wan, Y. Mi, and S. Ye, "Optimum control strategy of drive torque for pure electric vehicles during acceleration", *Journal of Jiangsu University (Natural Science Edition)*, 38(1), 1–6 (2017).

[18] J. Manton, "A Primer on Stochastic Differential Geometry for Signal Processing", *IEEE Journal of Selected Topics in Signal Processing* 7(4), 681–699 (2013).

[19] J. Manton, D. Applebaum, S. Ikeda, and N. Bihan, "Introduction to the issue on differential geometry in signal processing", *IEEE Journal of Selected Topics in Signal Processing* 7(4), 573–575 (2013).

[20] W. Huang, M. Yu, W. Fu, Y. Fan, Q. Wang, and P. Sun, "Analysis of influencing factors on testing results of vehicle roller anti-force brake testing platform" *Journal of Jiangsu University (Natural Science Edition)* 37(4), 497–502 (2017).

[21] Y. Huang, S. Fard, M. Khazraee, H. Wang, and A. Khajepour, "An adaptive model predictive controller for a novel battery-powered anti-idling system of service vehicles", *Energy* 127, 318–327 (2017).

[22] Y. Huang, A. Khajepour, F. Bagheri, M. Bahrami, and J. Yan, "Optimal energy-efficient predictive controllers in automotive air-conditioning/refrigeration systems", *Applied Energy*, 184, 605–618 (2016).

[23] G. Liu, L.Chen, W.Zhao, Y. Jiang, and L. Qu, "Internal Model Control of Permanent Magnet Synchronous Motor Using Support Vector Machine Generalized Inverse", *IEEE Transactions on Industrial Informatics* 9(2), 890–898 (2013).

[24] R. Zhong, Y. Xu, Y. Cao, X. Guo, W. Hua, S. Xu, and W. Sun, "Accurate model of switched reluctance motor based on indirect measurement method and least square support vector machine", *IET Electric Power Applications* 10(9), 916–922 (2016).

[25] Z. Li, W. Wang, X. Xu, and K. Jiang, "Willans model of electric motor for electric vehicle based on least squares support vector machine", *Journal of Jiangsu University (Natural Science Edition)* 37(4), 381–385 (2016).

[26] S. Vazquez, J. Gomez, J. Gamazo, and J. Femando, "A New Method for Sensorless Estimation of the Speed and Position in Brushed DC Motors Using Support Vector Machines", *IEEE Transactions on Industrial Electronics* 59(3), 1397–1408 (2012).

[27] C. Rojas, J. Rodriguez, S. Kouro, and F. Villarroel, "Multiobjective Fuzzy-Decision-Making Predictive Torque Control for an Induction Motor Drive", *IEEE Transactions on Power Electronics* 32(8), 6245–6260 (2017).

[28] R. Sun, R. Song, and K.Tong, "Complexity Analysis of EMG Signals for Patients After Stroke During Robot-Aided Rehabilitation Training Using Fuzzy Approximate Entropy", *IEEE Transactions on Neural Systems and Rehabilitation Engineering* 22(5), 1013–1019 (2014).

[29] K. Tan, "Squirrel-Cage Induction Generator System Using Wavelet Petri Fuzzy Neural Network Control for Wind Power Applications", *IEEE Transactions on Power Electronics* 31(7), 5242–5254 (2016).

[30] C. Li and L. Wu, "Sliding mode control for synchronization of fractional permanent magnet synchronous motors with finite time", *Optik-International Journal for Light and Electron Optics* 127(6), 3329–3332 (2016).
[31] J. Yang, M. Dou, and D. Zhao, "Iterative sliding mode observer for sensorless control of five-phase permanent magnet synchronous motor", *Bull. Pol. Ac.: Tech.* 65 (6), 845–857 (2017).
[32] Y. Huang, A. Khajepour, H. Ding, F. Bagheri, and M. Bahrami, "An energy-saving set-point optimizer with a sliding mode controller for automotive air-conditioning/refrigeration systems", *Applied Energy* 188, 576–585 (2017).
[33] R. Khanna, Q. Zhang, W. Stanchina, G. Reed, and Z. Mao, "Maximum Power Point Tracking Using Model Reference Adaptive Control", *IEEE Transactions on Power Electronics* 29(3), 1490–1499 (2014).
[34] C. Aguila and M. Duarte, "Improving the control energy in model reference adaptive controllers using fractional adaptive laws", *IEEE/CAA Journal of Automatica Sinica* 3(3), 332–337 (2016).
[35] P. Parenti, M. Leonesio, and G. Bianchi, "Model-based adaptive process control for surface finish improvement in traverse grinding", *Mechatronics* 36, 97–111 (2016).
[36] H. Jiang, C. Li, S. Ma, S. Ding, and C. Zhang, "Path tracking control of automatic parking for intelligent vehicle based on non-smooth control strategy", *Journal of Jiangsu University (Natural Science Edition)* 38(5), 497–502 (2017).
[37] H. Yu, T. Chen, and C. Liu, "Adaptive Fuzzy Logic Proportional-Integral-Derivative Control for a Miniature Autofocus Voice Coil Motor Actuator With Retaining Force", *IEEE Transactions on Magnetics* 50(11), 1–4 (2014).
[38] F. Lin, I. Sun, K. Yang, and J. Chang, "Recurrent Fuzzy Neural Cerebellar Model Articulation Network Fault-Tolerant Control of Six-Phase Permanent Magnet Synchronous Motor Position Servo Drive", *IEEE Transactions on Fuzzy Systems* 24(1), 153–167 (2016).
[39] A. Rubaai and P. Young, "Hardware/Software Implementation of Fuzzy-Neural-Network Self-Learning Control Methods for Brushless DC Motor Drives", *IEEE Transactions on Industry Applications* 52(1), 414–424 (2016).
[40] F. Sousy, "Intelligent Optimal Recurrent Wavelet Elman Neural Network Control System for Permanent-Magnet Synchronous Motor Servo Drive", *IEEE Transactions on Industrial Informatics* 9(4), 1986–2003 (2013).
[41] X. Diao and H. Zhu, "Survey of decoupling control strategies for bearingless synchronous reluctance motor", *Journal of Jiangsu University (Natural Science Edition)* 38(6), 687–695 (2017).
[42] T. Shi, Z. Qiao, C. Xia, H. Li, and Z. Song, "Modeling, analyzing, and parameter design of the magnetic field of a segmented halbach cylinder", IEEE Transactions on Magnetics 48(5), 1890–1898 (2012).
[43] G. Pathak, B. Singh, and B. Panigrahi, "Back-Propagation Algorithm-Based Controller for Autonomous Wind–DG Microgrid", *IEEE Transactions on Industry Applications*, 52(5), 4408–4415 (2016).
[44] B. Singh and S. Arya, "Back-Propagation Control Algorithm for Power Quality Improvement Using DSTATCOM", *IEEE Transactions on Industrial Electronics* 61(3), 1204–1212 (2014).
[45] H. Li, Q. Li, and J. Bai, "Automatic Control Systems of Electric Drive", *China Machine Press*, 2009.
[46] P. Gillella, X. Song, and Z. Sun, "Time-Varying Internal Model-Based Control of a Camless Engine Valve Actuation System", *IEEE Transactions on Control Systems Technology* 22(4), 1498–1510 (2014).
[47] Y. He, S. Zheng, and J. Fang, "Start-up current adaptive control for sensorless high-speed brushless DC motors based on inverse system metnod and internal mode controller", *Chinese Journal of Aeronautic*s 30(1), 358–367 (2017).
[48] X. Sun, Z. Shi, L. Chen, and Z. Yang, "Internal model control for a bearingless permanent magnet synchronous motor based on inverse system method", *IEEE Transaction on Energy Conversion* 31(4), 1539–1548 (2016).
[49] X. Sun, L. Chen, Z. Yang, and H. Zhu, "Speed-sensorless vector control of a bearingless induction motor with artificial neural network inverse speed observer", *IEEE/ASME Transactions on Mechatronics* 18(4), 1357–1366 (2013).
[50] S. Li and H. Gu, "Fuzzy Adaptive Internal Model Control Schemes For PMSM Speed-Regulation System", *IEEE Transactions on Industrial Informatics* 8(4), 767–779 (2012).